The paper was presented at the Tenth Meeting
"New Trends in Fatigue and Fracture" (NT2F10)
Metz, France, 30 August–1 September, 2010

Mohamed Hadj Meliani [1,2], Zitouni Azari [2], Guy Pluvinage [2], Yuri G. Matvienko [3]

TWO-PARAMETER FRACTURE CRITERION BY VOLUMETRIC METHOD APPROACH
DVOPARAMETARSKI KRITERIJUM LOMA PRISTUPOM VOLUMETRIJSKOG METODA

Original scientific paper
UDC: 621.643.2 : 539.42
Paper received: 31.01.2011

Author's address:
[1)] LPTPM, FSSI, Hassiba Ben Bouali University of Chlef, Esalem City, Chlef, Algeria, hadjmeliani@univ-metz.fr
[2)] Laboratoire de Mécanique, Biomécanique, Polymères, Structures, LaBPS-ENIM, Université Paul Verlaine de Metz, France
[3)] Laboratory of Modelling Damage and Fracture, Mechanical Engineering Research Institute of the Russian Academy of Sciences, Moscow, Russia

Keywords
- notch stress intensity factor
- effective distance
- master curve
- volumetric method

Ključne reči
- faktor intenziteta napona zareza
- efektivno rastojanje
- master kriva
- volumetrijska metoda

Abstract

A two-parameter fracture criterion has been proposed to predict fracture conditions of notched components. This criterion includes the critical notch stress intensity factor $K_{\rho,c}$ which represents fracture toughness of a material with a notch of radius ρ, and the non-vanishing parameter from the Williams equation, A_3 term. The effective A_3 -term A_{3eff} has been estimated as the average value of the A_3 term distribution in the region ahead of the notch tip at the effective distance X_{ef}. These parameters are derived from the volumetric method of notch fracture mechanics. The material failure curve or master curve $K_{\rho,c} = f(A_{3eff,c})$ is established as a result of notched specimen tests. It is shown that the notch fracture toughness is a linear decreasing function of the $A_{3eff,c}$ -stress. The use of the material failure curve to predict fracture conditions is demonstrated on gas pipes with the longitudinal surface notch.

Izvod

Predložen je dvoparametarski kriterijum loma za procenu uslova loma kod komponenata sa zarezom. Ovaj kriterijum sadrži kritični faktor intenziteta napona zareza $K_{\rho,c}$ koji predstavlja žilavost loma materijala sa zarezom radijusa ρ, i ne iščezavajući parametar iz jednačine Vilijemsa, član A_3. Efektivni član A_3, A_{3eff} je procenjen kao prosečna vrednost raspodele člana A_3 u oblasti ispred vrha zareza, na efektivnom rastojanju X_{ef}. Ovi parametri su izvedeni volumetrijskom metodom iz mehanike loma zareza. Kriva otkaza materijala ili master kriva $K_{\rho,c} = f(A_{3eff,c})$ je određena iz rezultata ispitivanja zarezanih epruveta. Pokazuje se da je žilavost loma zareza linearno opadajuća funkcija napona $A_{3eff,c}$. Upotreba krive otkaza materijala radi procene uslova loma data je na primeru gasnog cevovoda sa podužnim površinskim zarezom.

INTRODUCTION

For brittle mode I fracture in mainly elastic regime, current fracture assessment methodology relies on plane strain fracture toughness, K_{IC}, which is assumed to be a material property /1-4/. Recent studies /5-10/ have shown that fracture toughness can be strongly affected by specimen size, crack depth and loading configuration. This dependency is often referred to the effect of crack-tip constraint. However, the fracture toughness estimated from standard test specimens may lead to unduly conservative results. It is commonly accepted that standard specimens in laboratory testing are typically of high constraint while non-standard specimens and actual cracked structures may be low constraint configurations. The ASTM E-399 /11/ testing procedure recommends certain types of specimen geometries and K_{IC} can be considered as the plane-strain fracture toughness. All specimen geometries recommended by ASTM E-399 are high constraint. Using the recommendation specimen geometry for testing creates an "ASTM Window" since their corresponding T or A_3 values are within a certain range. The A_3 quantifies the third term of

Williams stress field expansion /5/. A K_{IC} value is believed to represent a lower limiting value of fracture toughness and the ASTM E-399 may not be generally valid. Increasing the size of a specimen shifts the stress distribution closer to the K-stress. Consequently, larger specimens tend to possess better K-dominance. This may explain why a large specimen is better suited for ASTM fracture toughness K_{IC} testing in addition to the reason for the plastic zone size. This phenomenon limiting the recommendation of ASTM and can be explained using the analytical K–T or K–A_3 relation for common effects of specimen geometries.

For the discussion above, it is now well-known in fracture mechanics community that the single fracture parameter alone may not be adequate to describe the crack-tip condition. To address this problem, there has been a recent surge of interest in crack-growth behaviour under conditions of low crack-tip stress triaxiality. This paper exploited the K–A_3 crack approach which is derived from a rigorous asymptotic solution and is developed for a two-parameter fracture. With K as the driving force and A_3 a constraint parameter, this approach has been successfully used to quantify the constraints of notch-tip fields for various proposed geometry and loading configurations.

EXTEND OF SINGLE PARAMETER FRACTURE MECHANICS (SPFM)

Classical Theoretical Background and motivation

Many researchers have long advocated more pragmatic, engineering approach to assess the fracture integrity of cracked structures /13/. This approach requires that constraint in the test specimen approximate that of the structure to provide an "effective" toughness for use in a structural integrity assessment. The appropriate constraint is achieved by matching thickness and crack depth between specimen and structure.

The K–A_3 crack approach

A detailed stress analysis is carried out in the vicinity of the crack front, in order to emphasize the characteristics of the two dimensional stress field. Due to that fact that in mode I, the crack propagation is determined by the stress perpendicular to the crack, namely σ_{yy}, this stress component is dealt with in the analysis. The linear elastic Williams' series solution is used for describing the crack tip stress fields. Three terms of Williams' solution, quantified by two parameters, K for the intensity of the stress field, T and A_3 for the crack tip constraint, are studied and found to be sufficient for representing the crack tip stress distribution. Similar three term approach is used for the interpretation of brittle fracture under quasi-static conditions (Chao and Zhang /6/; Chao and Reuter /47/, Chao et al. /7, 8/; Liu and Chao /48/). Note that the model de RKR – model describing the micromechanism of brittle fracture due to Ritchie, Knott and Rice /49/ proposes that crack growth in brittle fracture takes place when tensile stress at a critical distance r_c ahead of the notch-tip reaches a critical value σ_c. The conventional relation for mode I fracture

$$K_I = K_{IC} \tag{1}$$

can be considered as a simple representation of the RKR model. In Eq. (1), the mode I stress intensity factor K_I describes the state of stress near the crack-tip and fracture toughness K_{IC} is a material parameter representing the critical conditions required for fracture initiation. Numerous authors consider that the critical stress failure as a very promising and convenient fracture criterion, especially for running cracks or cracks in pipes. The maximum tangential stress, is often assumed, takes place along the line of the initial crack. Since the T-stress vanishes in the tangential stress along this direction, its effect on initiation of brittle fracture is normally ignored. Ayatollahi et al. /50/ reveal that the maximum along $\sigma_{\theta\vartheta}$ is not always zero$_{\theta=0}$ and angular deviation can occur only for positive values of T-stress. When the T-stress is negative the maximum $\sigma_{\theta\vartheta}$ is always along in the direction of propagation, $_{\theta=0}$. In mode I, fracture occurs when the tangential stress $\sigma_{\theta\vartheta}$ at some point along $\theta_{\max}$ at a critical distance r_c from the crack-tip, exceeds the critical or maximum stress σ_c. The tangential stress $\sigma_{\theta\vartheta}$ near the tip is rewritten as

$$\begin{aligned}\sqrt{2\pi r}\cdot\sigma_{\theta\theta} = K_I\cos^3\frac{\theta}{2} + T\sqrt{2\pi r}\cdot\sin^2\theta + \\ +\frac{3}{4}A_3\sqrt{2\pi r}\cdot\left(5\cos\frac{\theta}{2}-\cos\frac{5\theta}{2}\right)\end{aligned} \tag{2}$$

we can note $K_{app} = \sigma_{\theta\theta}\sqrt{2\pi r}$, with K_{app} representing the apparent stress intensity factor. At fracture, critical apparent stress intensity factor $K_{app,c}$, using Eq. (2), one then has

$$\begin{aligned}K_{app,c} = (\sigma_{\theta\theta})_{\max}\sqrt{2\pi r_c} = K_c\cos^3\frac{\theta_c}{2} + T_c\sqrt{2\pi r_c}\cdot\sin^2\theta_c + \\ +\frac{3}{4}A_{3c}\sqrt{2\pi r_c}\cdot\left(5\cos\frac{\theta_c}{2}-\cos\frac{5\theta_c}{2}\right)\end{aligned} \tag{3}$$

For mode I, assuming three terms are sufficient to characterise the crack-tip stress field; we examine the case when crack dose not curve, i.e. the second term in Eq. (2) or the T-stress vanishes. Equation (3) becomes

$$K_{app} = \sigma_{\theta\theta,\theta=0}\sqrt{2\pi r} = K_I + 3\sqrt{2\pi}\cdot A_3\cdot r \tag{4}$$

The A_3 term in the Williams series expansion is determined by employing finite element analysis and Eq. (4) can be rewritten for high order as

$$K_{app} = \sigma_{\theta\theta,\theta=0}\sqrt{2\pi r} = K_I + B_3 r + B_5 r^2 \tag{5}$$

where $B_3 = 3\sqrt{2\pi}\,A_3$ and $B_5 = 5\sqrt{2\pi}\,A_5$. If the stress intensity factor distribution expressed by the left side of Eq. (5) is plotted against the distance from the crack-tip r, a linear fit to the data will yield the slope m. Then, A_3 can be obtained from the slope m, that is $A_3 = m/3\sqrt{2\pi}$. For the distribution of the stress intensity factor in Eq. (5), the fit is a parabolic curve. Having both K_{app} and A_3 determined the three term solutions in Eq. (4) give the near crack-tip stress.

Volumetric method mesofracture to extend SPFM to notch

Although many works have carried out estimation for the stress intensity factor with the presence of T-stress of pipeline, they have exclusively focused on classical fracture

mechanics with crack to estimate the toughness. We present notch fracture mechanics (NFM) principles applied to study stress distribution at the notch tip of pipes submitted to internal pressure. Volumetric Method, presented by Pluvinage /51/ is a meso-mechanical method belonging to this NFM. It is assumed, according to the mesofracture principle that the fracture process requires a physical volume. This assumption is supported by the fact that fracture resistance is affected by loading mode, structural geometry, and scale effect. By using the value of the "hot spot stress" i.e. the maximum stress value, it is not possible to explain the influence of these parameters on fracture resistance. It is necessary to take into account the stress value and the stress gradient in all neighbouring points within the fracture process volume. This volume is assumed to be quasi-cylindrical with a notch plastic zone of similar shape. The diameter of this cylinder is called the "effective distance". By computing the average value of stress within this zone, the fracture stress can be estimated, this leads to a local fracture stress criterion based on two parameters, the effective distance X_{eff} and the effective stress σ_{eff}, the graphical representation of this local fracture stress criterion is given in Fig. 1, where the stress normal to the notch plane is plotted against the distance ahead of notch. For determination of X_{eff}, a graphical procedure is used; it has been observed that the effective distance is related to the maximum value of the relative stress gradient χ. This distance corresponds to the beginning of the pseudo stress gradient is indicated in Fig. 2. The opening stress distribution at the notch is calculated using FEM for elastic analysis of 2D model in plane strain conditions, the effective distance X_{eff} is determined using normal stress distributions below. The notch root, plotted in bi-logarithmic axes; the relative stress gradient (see Eq. (6)), plotted on the same graph, allows obtaining an effective distance precise value.

$$\chi(r)=\frac{1}{\sigma_{yy}(r)}\frac{\partial\sigma_{yy}(r)}{\partial r} \tag{6}$$

where $\chi(r)$and $\sigma_{yy}(r)$ are the relative stress gradient and maximum principal stress or crack opening stress, respectively. The relative stress gradient depicts the severity of the stress concentration around the notch and crack tips. However, the stress distribution effect is not solely a major parameter for the fracture process zone. The minimum point of the relative stress gradient in the bi-logarithmic diagram is conventionally taken into account as the relevant effective distance and signifies the virtual crack length. The effective stress is defined as the average of the weighted stress inside the fracture process zone:

$$\sigma_{eff}=\frac{1}{X_{eff}}\int_0^{X_{ef}}\sigma_{yy}(r)\Phi(r)dr \tag{7}$$

where σ_{eff}, X_{eff}, $\sigma_{yy}(r)$ and $\Phi(r)$ are effective stress, effective distance, maximum principal stress and weight function, respectively. The unit weight function and Peterson's weight function are the simplest definitions of weight function the effective distance. The unit weight function deals with the average stress and Peterson's weight function gives the stress value at a specific distance and it is not required to compute numerical integration. Therefore, the noted Notch Stress Intensity Factor, NSIF, is described and is defined as a function of effective distance and effective stress given by relationship

$$K_\rho=\sigma_{eff}\sqrt{2\pi X_{eff}} \tag{8}$$

the NSIF is considered as a value of facture toughness with units MPa·m$^{0.5}$, and the minimum effective distance corresponds to the abscissa of the upper limit of zone II and its distance from notch root is suggested to be the effective distance X_{eff}. The effective T-stress, T_{eff} is not singular as $r\to0$, but it can modify to the effective crack tip plastic zone. T_{eff} can be rewritten as

$$T_{eff}=\frac{1}{X_{eff}}\int_0^{X_{eff}}T_{xx}(r)\Phi(r)dr \tag{9}$$

with $T_{xx}=(\sigma_{xx}-\sigma_{yy})$ and the effective stress intensity factors take the form of

$$K_{eff}=K_\rho+T_{eff}\sqrt{2\pi X_{eff}}=\sigma_{eff}\sqrt{2\pi X_{eff}}+T_{eff}\sqrt{2\pi X_{eff}}$$
$$\text{as } r\to X_{eff} \tag{10}$$

and the stress biaxiality ratio in the effective distance can by rewritten as

$$\beta_{eff}=\frac{T_{eff}\sqrt{2\pi X_{eff}}}{K_\rho} \tag{11}$$

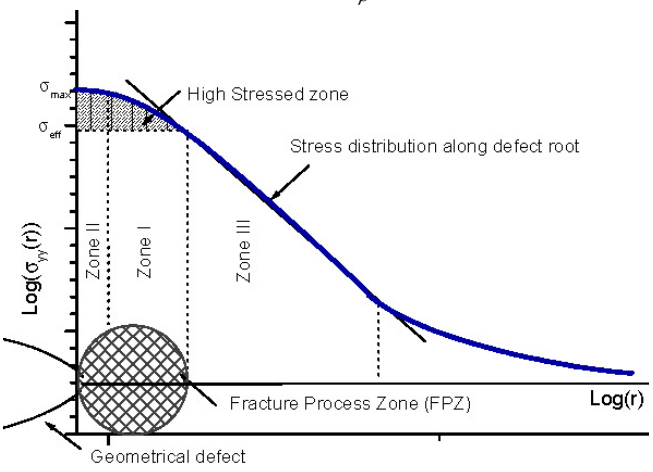

Figure 1. Schematic presentation of a local stress criterion for fracture emanating from notches.
Slika 1. Shema kriterijuma lokalnog napona za lom koji potiče od zareza

The Notch Stress Intensity Factor K_ρ, the effective T-stress, T_{eff}, near the notch root and the relative distance are shown in Fig. 2. Effective T-stress is used as constraint parameter. This addition to the classical plastic notch tip parameter K_ρ provides an effective two-parameter characterization of elastic notch-tip fields in a variety of notch configurations and loading conditions. With the volumetric method, we examine the case when crack does not curve, i.e. the second term in Eq. (3) or the T-stress vanishes. Equation (4) becomes

$$K_{eff}^{c}=\sigma_{\theta\theta,\theta=0}\sqrt{2\pi X_{eff}}=K_\rho+3\sqrt{2\pi}\cdot A_{3eff}\cdot r \tag{12}$$

The A_{3eff} term in the Williams' series expansion is determined by finite element analysis.

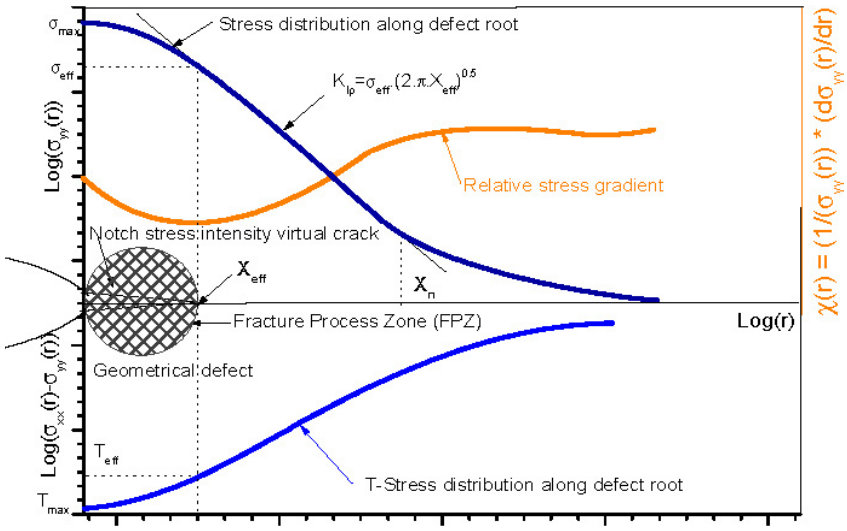

Figure 2. Determination of effective stress intensity factor and the effective T-stress at notch root together with the relative stress gradient versus distance from the notch tip.
Slika 2. Određivanje efektivnog faktora intenziteta napona i efektivnog T-napona u korenu zareza zajedno sa relativnim gradijentom napona u zavisnosti od rastojanja od vrha zareza

Finite Element Modelling

The geometry considerate in this study is a cylinder with a V-shaped longitudinal surface notch subject to different internal pressure P, as shown in Fig. 3. The effect of three parameters: ratio of inner radius of the cylinder to the thickness, R_i/t, the ratio of the notch depth to cylinder thickness, a/t, and pressure on T-stress and Stress Intensity factors (SIF) is systematically considered. To cover practical and interesting ranges of these three variables, four different values of R_i/t, 5, 10, 20 and 40, are selected. In terms of crack depth, four different values of a/t are selected, ranging from $a/t = 0.1$ to 0.75. In terms of pressure, four different values of p are selected, ranging from pressure of 20 to 50 bar. Thus, a total of 84 different experimental setups are considered in this investigation, the details of which are listed in Table 1.

The finite element method is used to determine notch-tip parameters T and SIF for the pipe specimens. The structure are modelled by CASTEM 2000 code in two dimensions under plane strain conditions using free meshed isoperimetric triangulateral elements only on half of the specimen. The elastic analyses comprise 31485 elements and 63526 nodes. A fanlike mesh focused at the notch-tip is employed, because this yields more accurate non-singular terms estimates. Further, a more detailed mesh sensitivity study has shown that further refinement of the mesh leads to only small changes (< 1%), the pipe specimen geometry is illustrated in Fig. 3. The wall thickness is 10 mm, the length of the pipe is 40 mm, dimensions of the notch are presented in Fig. 4a. Support and symmetric boundary conditions are used in this model.

Table 1. List of analysis cases for the FE analysis.
Tabela 1. Skup slučajeva za FE analizu

P	R_i/t	a/t	P	R_i/t	a/t	P	R_i/t	a/t	P	R_i/t	a/t
20	5	0.1	20	10	0.1	20	20	0.1	20	40	0.1
		0.3			0.3			0.3			0.3
		0.5			0.5			0.5			0.5
		0.75			0.75			0.75			0.75
30	5	0.1	30	10	0.1	30	20	0.1	30	40	0.1
		0.3			0.3			0.3			0.3
		0.5			0.5			0.5			0.5
		0.75			0.75			0.75			0.75
40	5	0.1	40	10	0.1	40	20	0.1	40	40	0.1
		0.3			0.3			0.3			0.3
		0.5			0.5			0.5			0.5
		0.75			0.75			0.75			0.75
50	5	0.1	50	10	0.1	50	20	0.1	50	40	0.1
		0.3			0.3			0.3			0.3
		0.5			0.5			0.5			0.5
		0.75			0.75			0.75			0.75

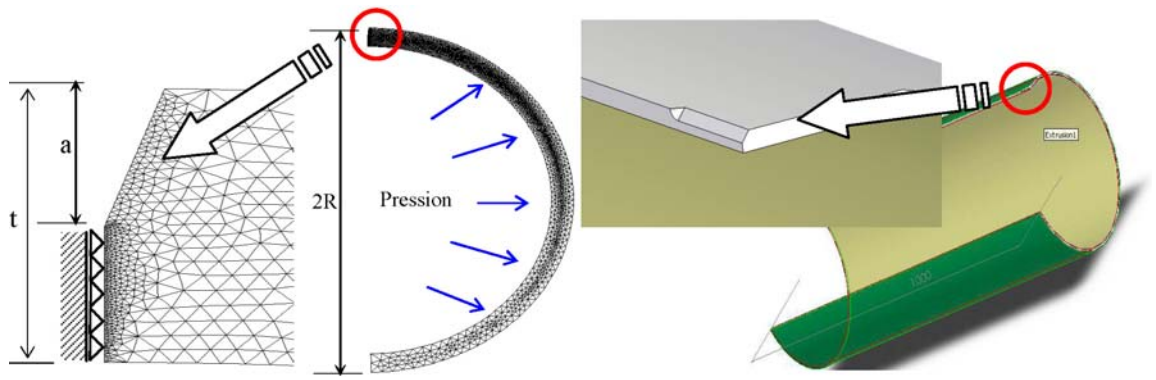

Figure 3. (a) Geometry boundary conditions and loading configuration using the half of pipe. (b) Typical 2D finite element mesh used to model the crack on the half pipeline for elastic analysis.
Slika 3. (a) Geometrija graničnih uslova i konfiguracija opterećenja za jednu polovinu cevi. (b) Tipična 2D mreža konačnih elemenata za modeliranje prsline na polovini cevovoda za elastičnu analizu

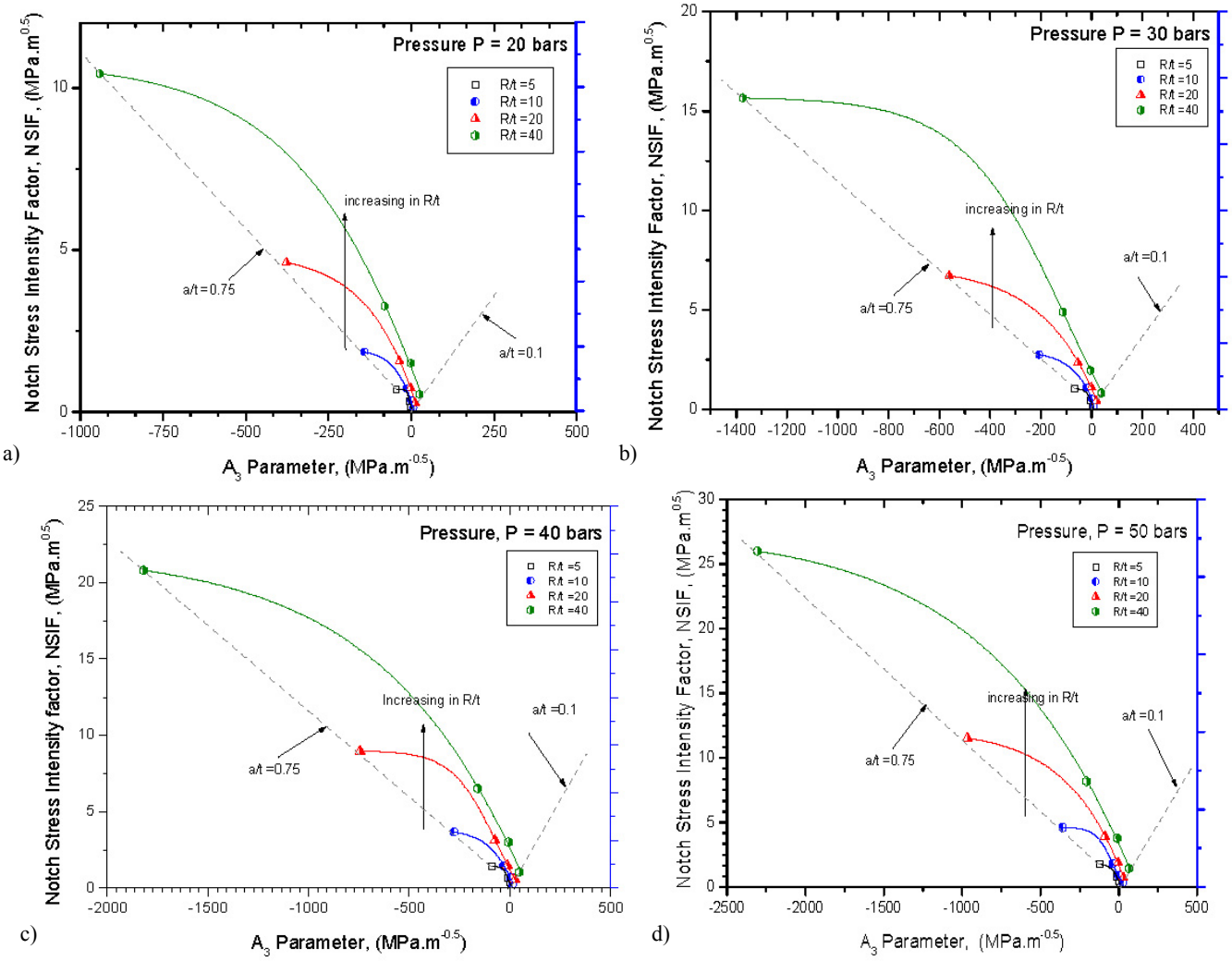

Figure 4. Development of notch tip constraint represented by A_3 for various situations of pressure and diameters of Pipeline.
Slika 4. Razvoj veze na vrhu zareza predstavljeno sa A_3 za razne slučajeve pritiska i prečnika cevovoda

INTERPRETATION OF RESULTS AND DISCUSSION

A detailed stress analysis is carried out in the vicinity of the notch front, in order to emphasize the characteristics of the two-dimensional stress field. Due to the fact that in Mode I, crack propagation is determined by the stress perpendicular to the notch, namely σ_{yy}, this stress component is dealt within the analysis. The coefficients of the higher order stress terms represent one part of a larger database which shall also include information on various constraint parameters. Since this study is concentrated on elastic two-dimensional notches and initial part of the finite element constraint parameter are investigated.

Recently, some publications have carried out a complete analysis of higher order crack fields in power-law hardening materials and have shown that a two-term expansion is not sufficient to describe the near tip fields while more than three terms are redundant. In this application, the effects of pipeline size, loading configuration and notch depth are presented.

In order to investigate the effect of pressure on the constraint for notch-tip field, the developments of Notch Stress Intensity Factors at different pressure (P = 20, 30, 40 and 50 bar) are modelled and the results are shows in Fig. 4a-d. The data on K_ρ versus A_3 are plotted on different diameters (R/t = 5, 10, 20 and 40). The first remarks that K_ρ increase with increasing $-A_3$. For small notch length, $a/t < 0.3$, the values of A_3 are positive for all pressure and pipe diameters. Since a pipe has large a/t ratios, this parameter takes very negative values. It can be seen that A_3 has a linear function a/t, and increases with increasing the depth of the notch and pressure (see Fig. 5 for example). This observation is in contradiction with the remarks of Lam et al. /52/. The authors /52/ justified the constants value of A_3 when the pressure increases by the Large Scale Yielding (LSY) condition.

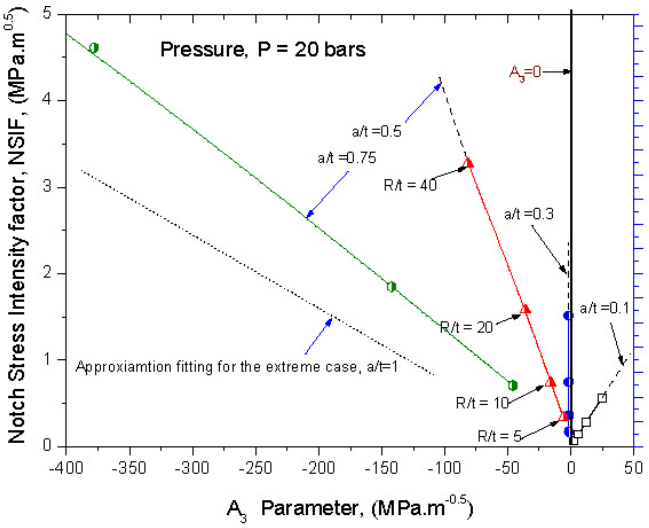

Figure 5. Example of linear relationship between the A_3 parameter and the pipe diameter for different a/t (P = 20 bar).
Slika 5. Primer linerane veze parametra A_3 i prečnika cevovoda za različite a/t (P = 20 bar)

Figure 6 shows the situation of the higher order terms near the crack-tip. In this work we only consider the opening stress along the zero degree direction ahead of the notch tip. That is, we assumed that the crack would propagate along the zero degree direction. For any flawed specimen or structure, a notch driving force may be established by running a linear elastic FEA for the geometry and any applied load to determine the pair (K_ρ, A_3). For a surface notch, the crack front is a curved line. A (K_ρ, A_3) pair and a notch driving force at each point along the notch front are present as the far field load is increased. By putting the entire notch driving forces along the notch front together, the notch driving force for the surface notch becomes a curved front as depicted in Fig. 7.

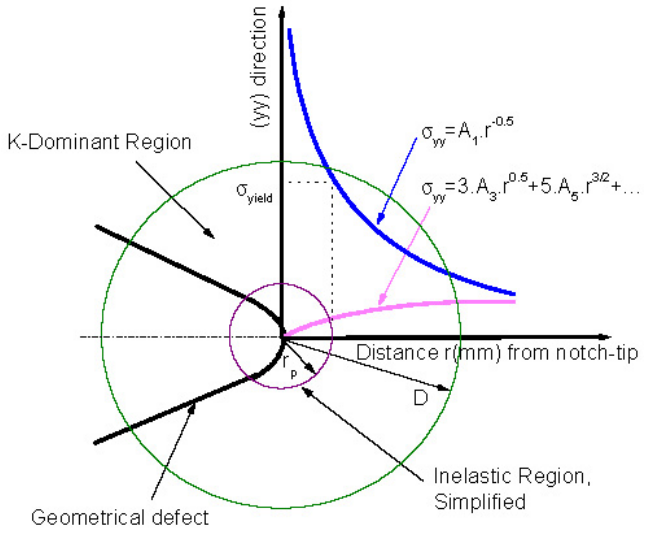

Figure 6. The concept of the extended SFEM.
Slika 6. Koncepcija proširene SFEM

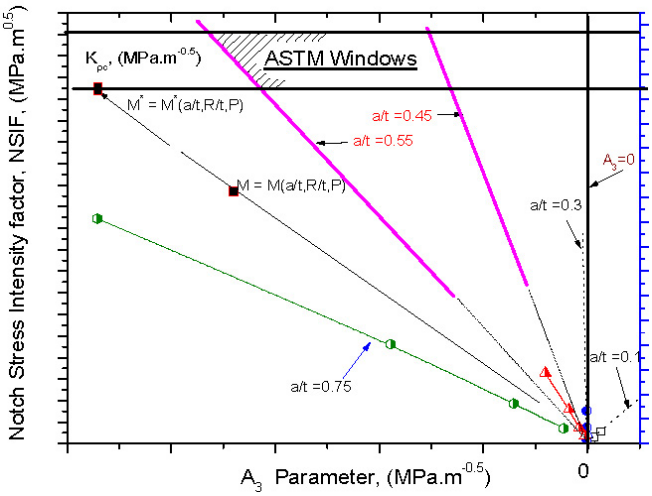

Figure 7. Schematic presentation of A_3 variation versus NSIF.
Slika 7. Shematski prikaz promene A_3 sa NSIF

Since (K_ρ, A_3) varies from point to point along the notch front for a given far field load. Each point on the curve represents the condition of the opening stress at a particular point in the notch front of the surface crack. For instance, the left point of the curve may represent the condition of the opening stress at the deepest point of the surface notch and the right point corresponding to the point where the crack front intersects with the surface.

For common specimen geometries, the relation between K and A_3 is tabulated from numerical calculations for convenience. Since the ratio between K and A_3 is a constant for a given geometry. In Fig. 7, point (0,0) represents the condition of no applied load. The two points (0,0) and (K–A_3) from the driving force represented in a straight line in the K–A_3 plane and the intersection of the notch driving force with the material failure line yields the predicted K_C and A_{3C} for the particular flawed structure.

CONCLUSIONS, REMARKS

The K–A_3 methodology is used and A_3 parameter is identified to quantify the constraint at the notch tip. Procedures to shift the mechanical properties curve between Pipelines of different in-plane constraint levels are developed which enables the determination of the transition curve of non-standard flawed structures from the experimental results of standard specimens. The magnitudes of negative A_3 parameters are greater than those of large diameters of pipelines. The low constraint due to relatively large magnitude of negative A_3 term may be expected to inhibit the crack extension in the same plane and promote crack kinking. Further, among the small diameters, the less A_3 exhibit lower apparent K.

REFERENCES

1. Williams, M.L., *On the stress distribution at the base of stationary crack*, ASME J Appl Mech 1957; 24 : 109-114.
2. Rice, J.R., *Limitations to the-scale yielding approximation for crack-tip plasticity*, J Mech. Solids, 22, 17-26 (1974).
3. Larsson, S.G., Carlsson, A.J., *Influence of non-singular stress terms and specimen geometry on small-scale yielding at crack tips in elastic-plastic materials*, J Mech. Phys. Solids 21, 263-278 (1974).
4. Leevers, P.S., Radon, J.C., *Inherent stress biaxiality in various fracture specimen geometries*, Int. J Fract. 19, 311-325 (1982).
5. Richardson, D.E., A new biaxial stress fracture criterion, PhD dissertation, Clemson University (1991).
6. Chao, Y.J., Zhang, X., *Constraint effect in brittle fracture*, 27th National Symposium on Fatigue and Fracture, ASTM STP 1296, R.S. Piascik, J.C. Newman, Jr. and D.E. Dowling, Eds., American Society for Testing and Materials, Philadelphia, pp.41-60 (1997).
7. Chao, Y.J., Liu, S., Broviak, B.J., *Variation of fracture toughness with constraint of PMMA specimens*, Proceedings of ASME-PVP Conference 393, 113-120 (1999).
8. Chao, Y.J., Liu, S., Broviak, B.J., *Brittle fracture: variation of fracture toughness with constraint and crack curving under mode I conditions*, Experimental Mechanics 41(3), 232-241 (2001).
9. Smith, D.J., Ayatollahi, M.R., Pavier, M.J., *The role of T-stress in brittle fracture for linear elastic materials under mixed mode loading*, Fatigue and Fracture of Engineering Materials and Structures 24(2), 137-150 (2001).
10. Ayatollahi, M.R., Pavier, M.J., Smith, D.J., *Mode I cracks subjected to large T-stresses*, Int. J of Fracture 117(2), 159-174 (2002).
11. ASTM E399, Standard Test Methods for Plane-Strain Fracture Toughness of Metallic Materials, Annual Book of ASTM Standards, Vol.03.01.
12. Willis, J.R., *Asymptotic analysis in fracture: An update*, Int. J of Fracture, 100:85-103, 1999.
13. Dawes, M.G., Pisarski, H.G., Towers, O.L., Williams, S., *Fracture mechanics measurements of toughness in welded joints*, Fracture Toughness Testing: Methods, Interpretation, and Application, TWI, Cambridge, UK, pp.165-178, 1982.
14. Sumpter, J.D.S., *An experimental investigation of the T stress approach*, Constraint effects Fracture, ASTM STP 1171 (Eds. E.M. Hackett, K.-H. Schwalbe, R.H. Dodds), ASTM, Philadelphia, 492-502, 1993.
15. Kirk, M.T., Dodds, R.H.J., *CTOD estimation equations for shallow cracks in single edge notch bend specimens*, Shallow crack fracture mechanics, toughness tests and applications. TWI 1992. Paper 2.
16. Mark, T., Kirk, *The Second ASTM/ESIS Symposium on Constraint Effects in Fracture; an Overview*, Int. J Pres. Vls. & Piping 64 (1995), 259-275.
17. Nakamura, T., Parks, D.M., *Determination of elastic T-stress along three-dimensional crack fronts using an interaction integral*, Int. J Solids Struct. 29: 1597-611 (1991).
18. Bilby, B.A., Cardew, G.E., Goldthorpe, M.R., Howard, I.C.A., *Finite element investigation of the effect of specimen geometry on the fields of stress and strain at the tips of stationary cracks*, In: Size effects in fracture, London: Mechanical Engineering Publications Limited. p.37-46 (1986).
19. Betegon, C., Hancock, J.W., Two-parameter characterization of elastic plastic crack tip fields, ASME J Appl Mech. 58:104-110 (1991).
20. Du, Z.Z., Hancock, J.W., *The effect of non-singular stresses on crack tip constraint*, J Mech Phys Solids, 39: 555-67 (1991).
21. Cotterell, B., *Notes on the paths and stability of cracks*, Int. J of Fracture Mechanics 2, 526-533 (1966).
22. Cotterell, B., *On fracture path stability in the compact tension test*, Intern. J of Fracture Mechanics 6, 189-192 (1970).
23. Melin, S., *Why do cracks avoid each other?*, Int. J Fract. 23, 37-45.
24. Marder, M., *Instability of crack in a heatep strip*, Physical Review E. Vol 49, N1, 49-53.
25. Yuse, A., Sano, M., Nature (London) 362, 329 (1993).
26. Cotterell, B., Rice, J.R., *Slightly curved or kinked cracks*, Int. J Fract. 16, 155-169 (1980).
27. Selvarathinam, A.S., Goree, J.G., *T-stress based fracture model for cracks in isotropic materials*, Engineering Fracture Mechanics 60, 543-561 (1998).
28. Ramulu, Kobayashi, A.S., *Dynamic Crack Curving: A Photoelastic Evaluation*, Exp. Mechanics, Vol.23, pp.1-9 (1983).
29. Ravi-Chandar, K., Knauss, W.G., *An Experimental Investigation into Dynamic Fracture: III. On Steady-state Crack Propagation and Crack Branching*, Int. J of Fracture, Vol.26, pp.141-154; 198-200 (1984).
30. Knauss
31. Fleck, N.A., Hutchinson, J.W., Suo, Z., Crack path selection in a brittle adhesive layer, Int. J of Solids and Structures 27, 1683-1703 (1991).
32. Banks-Sills, Schwartz, J., *Fracture testing of Brazilian disk sandwich specimens*, Int. J of Fracture 118: 191-209, 2002.
33. Larsson, S.G., Carlsson, A.J., *Influence of non-singular stress terms and specimen geometry on small-scale yielding at crack tips in elastic-plastic materials*, J Mech. Phys. Solids 21, 263-278 (1973).
34. Rice, J.R., *Limitations to the-scale yielding approximation for crack-tip plasticity*, J Mech. Solids, 22, 17-26 (1974).
35. Kirk, M.T., Koppenhoefer, K.C., Shih, C.F., *Effect of constraint on specimen dimensions needed to obtain structurally relevant toughness measures*, Constraint in Fracture, ASTM STP 1171 (Eds. E.M. Hachett, K.-H. Schwalbe, R.H. Dodds), ASTM, Philadelphia, 79-103 (1993).
36. Sorem, W.A., Dodds, R.H., Rolfe, S.T., *Effects of crack depth on elastic plastic fracture toughness*, Int. J of Fracture 47, 105-126 (1991).
37. Hancock, J.W., Reuter, W.G., Parks, D.M., *Constraint and toughness parameterized by T*, Constraint Effects in Fracture, ASTM STP 1171 (Eds. E.M. Hackett, K.-H. Schwalbe, R.H. Dodds), ASTM, Philadelphia, 21-40 (1993).
38. Sumpter, J.D.S, *An experimental investigation of the T stresses approach*, Constraint Effects in Fracture, ASTM STP 1171 (Eds. E.M. Hackett, K.-H. Schwalbe, R.H. Dodds), ASTM, Philadelphia, 492-502 (1993).
39. Ganti, Parks, D.M., *Elastic .plastic fracture mechanics of strength-mismatch interface cracks*, In: Mahudhara R.K. et al.,

eds. Recent Advances in Fracture, London: The Minerals, Metals and Material Society, p.13-25 (1997).
40. Zhang, Z.L., Hauge, M., Taulow, C., *The effect of T -stress on the near tip stress field of an elasticplastic interface crack*, In: Karihaloo, B.L. et al., eds., Proc. of the Ninth Intern. Conf. on Fracture, Vol.4, Amsterdam, Pergamon, p.2643-50 (1997).
41. Li, X.F., Xu, L.R., *T-stresses across static crack kinking*, J Appl. Mech., in press.
42. Melin, S., *The influence of the T-Stress on the directional stability of cracks*, Int. J Fract., 2002; 114:259-265.
43. Richardson, D.E., Goree, J.G., *Experimental verification of a new two parameter fracture model*, Fracture mechanics: twenty-third symposium, ASTM STP 1189, 1993. p.738-50.
44. Richardson, D.E., Rapport de nasa
45. Yang, B., Ravi-Chandar, K., *Evaluation of elastic T-stress by the stress difference method*, Engng. Fract. Mech. 64:589-605 (1999).
46. Leevers, P.S., Radon, J.C., *Inherent stress biaxiality in various fracture specimen geometries*, Int. J Fract. 19, 311-325 (1982).
47. Chao, Y.J., Reuter, W.G., *Fracture of surface cracks under bending loads*, In: Underwood J.H., MacDonald, B., Mitchell, M. (eds.), Fatigue and Fracture Mechanics, Vol.28, ASTM STP 1321, ASTM, Philadelphia, pp.214-242 (1997).
48. Liu, S, Chao, Y.J., *Variation of fracture toughness with constraint*, Int. J Frac. 124:113-117 (2003).
49. Ritchie, R.O., Knott, J.F., Rice, J.R., *On the relationship between critical tensile stress and fracture toughness in mild steel*, J Mech. Physics Solids 21:395-410 (1973).
50. Ayatollah, M.R, Pavier, M.J, Smith, D.J., *Determination of T-stress from finite element analysis for mode I and mixed mode I/II loading*, Int. J of Fracture 91, 283-298 (1998).
51. Pluvinage, G., Fracture and Fatigue Emanating from Stress Concentrators, Kluwer Publisher, (2003).
52. Lam, P.S., Chao, Y.L., Zhu, X.Y., Kim, Y., Sindelar, R.L., *Determination of constraint-Modified J-R curves for carbon steel storage tanks*, J of Pressure and Vessel Technology, Vol.125 (2003).